TU Delft

Delft University of Technology

Evaluation of the sparse reconstruction and the delay-and-sum damage imaging methods for structural health monitoring under different environmental and operational conditions

Nokhbatolfoghahai, A.; Navazi, H. M.; Groves, R. M.

DOI
10.1016/j.measurement.2020.108495

Publication date
2021

Document Version
Final published version

Published in
Measurement: Journal of the International Measurement Confederation

Citation (APA)
Nokhbatolfoghahai, A., Navazi, H. M., & Groves, R. M. (2021). Evaluation of the sparse reconstruction and the delay-and-sum damage imaging methods for structural health monitoring under different environmental and operational conditions. *Measurement: Journal of the International Measurement Confederation*, *169*, Article 108495. https://doi.org/10.1016/j.measurement.2020.108495

Important note
To cite this publication, please use the final published version (if applicable).
Please check the document version above.

Copyright
Other than for strictly personal use, it is not permitted to download, forward or distribute the text or part of it, without the consent of the author(s) and/or copyright holder(s), unless the work is under an open content license such as Creative Commons.

Takedown policy
Please contact us and provide details if you believe this document breaches copyrights.
We will remove access to the work immediately and investigate your claim.

This work is downloaded from Delft University of Technology.
For technical reasons the number of authors shown on this cover page is limited to a maximum of 10.

Green Open Access added to TU Delft Institutional Repository

'You share, we take care!' - Taverne project

https://www.openaccess.nl/en/you-share-we-take-care

Otherwise as indicated in the copyright section: the publisher is the copyright holder of this work and the author uses the Dutch legislation to make this work public.

Measurement 169 (2021) 108495

Contents lists available at ScienceDirect

Measurement

journal homepage: www.elsevier.com/locate/measurement

Evaluation of the sparse reconstruction and the delay-and-sum damage imaging methods for structural health monitoring under different environmental and operational conditions

A. Nokhbatolfoghahai [a,b], H.M Navazi [a,*], R.M. Groves [b]

[a] Department of Aerospace Engineering, Sharif University of Technology, Azadi Ave., PO Box: 11155-8639, Tehran, Iran
[b] Aerospace Non-Destructive Testing Laboratory, Faculty of Aerospace Engineering, Delft University of Technology, 2628 CD Delft, the Netherlands

ARTICLE INFO

Keywords:
Structural health monitoring
Delay-and-sum
Sparse reconstruction
Taguchi method
Guided lamb wave

ABSTRACT

In this paper, the performance of the sparse reconstruction (SR) and the delay-and-sun (DAS) methods for damage localization, were evaluated for various environmental and operational conditions, both numerically and experimentally. To assess these damage localization methods, a methodology based on the Taguchi method was used to make the experimental design, and a modified performance-index was defined to represent the quality of reconstructed images. Then, the robustness and the accuracy of each method, in a well-defined performance region relevant to in-service aerospace structures, were investigated using the Taguchi and analysis of variance methods. It was concluded that for the defined conditions, the robustness of the delay and sum method is better than the sparse reconstruction method for uncontrolled factors. However, the sparse reconstruction method is more robust to poor baseline subtraction than the delay and sum method, while the delay and sum method was more robust to factors that lead to a model mismatch. These results provide additional insight into the design of reliable accurate structural health monitoring systems. The outcomes of this work can be used in future reaserch into SHM imaging techniques.

1. Introduction

Condition-Based Maintenance (CBM) of structures involves continuous real-time monitoring of the structure, and decision making to determine its current condition of the structure. This allows the operators to improve maintenance efficiency by enabling a move from scheduled maintenance to maintenance based on condition [1]. Structural Health Monitoring (SHM) can support these significant changes in the maintenance procedures

replacing the periodic and scheduled maintenance by real-time monitoring of the integrity of in-service structures [1].

To perform active SHM, guided Lamb waves have recently gained a lot of attention [2,3] as they can scan large areas of structures with a few sensors and are sensitive to barely-visible structural damages [4,5].

In guided Lamb-wave SHM, signal features e.g. amplitude, frequency and time of flight (TOF) changes [6], is used to identify the presence of damage followed by applying localization algorithms to find the damage location(s). Examples of localization algorithms are phase array approaches [7], the tomography technique [8], the semi-instantaneous baseline approach [9], the minimum variance method [10] and the Delay-and-Sum (DAS) algorithm [11]. Further steps would be to measure and to assess the effect of the damage on the structural integrity [12] and to preform prognosis of the remaining useful life of the structure.

The DAS method was developed by Wang *et al.* [11], and Michaels applied this method to the residual signal (subtraction of the baseline signal from the acquired signal) [13]. This method has received noticeable attention due to its simplicity and robustness [14,15] with regard to other methods. However, in some circumstances such as at the presence of multiple damages and with poor baseline subtraction, the performance of this method decreases due to a large spot size and high noise levels [16]. Furthermore, some previous research has evaluated and increased the performance of this method [17,18] and investigated the effect of operational conditions such as temperature and vibration on the performance of the DAS method [13,19].

Recently, Levine and Michaels [20,21] developed a new imaging method that is based on the assumption of the sparsity of structural damages and sparse reconstruction (SR). This method was applied to

* Corresponding author.
E-mail address: navazi@sharif.edu (H.M Navazi).

https://doi.org/10.1016/j.measurement.2020.108495
Received 30 April 2020; Received in revised form 27 August 2020; Accepted 19 September 2020
Available online 28 September 2020
0263-2241/© 2020 Elsevier Ltd. All rights reserved.

residual signals and is a dictionary-based approach that was successfully demonstrated to be applicable for the detection of scatters. Recently, Wang et al. [22] designed a comprehensive dictionary containing various waveforms under diverse conditions, and they validated its functionality by both metal beam and composite wind turbine experiments. Later, Hua et al. [23] proposed sparse reconstruction imaging for Lamb wave simultaneous excitation system to obtain both efficient data acquisition and high imaging performance. In addition, Xu et al. [24] developed a method based on weighted sparse reconstruction and Nokhbatolfoghahai et al. [25,26] demonstrated a hybrid DAS-SR method based on combination of the SR and DAS methods and weighted sparse-reconstruction, to improve the computational performance and robustness of both methods in case of multi damage presence and using low sampled signal.

Although, some researchers have demonstrated that the SR method has a high potential and have shown that the images reconstructed with the SR method were superior to the DAS method [21,27,28], they did not study the influence of possible limitations such as poor baseline subtraction or model mismatch, which could occur in realistic in-service operational and environmental conditions. Levine also emphasized the importance of further assessment into the robustness of this method in some operational conditions in [28].

Other previous research [29–32] has investigated the effects of operational conditions on SHM systems for damage detection and only a few studies have assessed imaging methods [19,33–36]. However these environmental parameters were only assessed individually and multi-parameter interactions were not studied.

In real operating conditions, uncertainty in some parameters cause model mismatch in SHM systems, such as existing unpredictable noise and lack of information about the exact mode of the Lamb wave propagation, while others reduce the quality of comparison for example temperature variation and humidity. Despite applying the compensation methods described in [34,37–40] and some methods for signal treatments such as sparse Bayesian learning [41,42], these factors continue to cause challenges and to decrease the accuracy and reliability of SHM methods.

To perform a multi-parameter assessment, a simple approach using a full factorial would require a large number of measurements. Therefore we use the Taguchi method as a robust and efficient Design of Experiment (DOE) method in this paper. Also, to use the proposed evaluation method for the first time, we have chosen a simple structure to reduced the uncontroled factors as much as possible.

This paper consists of an introduction to the algorithms used (Section 2), the developed methodology for the DOE (Section 3), a description of the design of the experimental setup and numerical models (Section 4), results, discussion and conclusions (Sections 5 and 6).

2. Theoretical background

This section, introduces the theory of Lamb waves, and the DAS and SR imaging methods.

2.1. Lamb waves

Lamb waves are a type of elastic wave that are guided between two parallel free surfaces of a thin-wall structure such as a plate or shell [3]. A propagating Lamb wave has two classes, symmetric (S_n) and anti-symmetric (A_n) modes. The symmetrical and antisymmetric zero-order modes (S_0 and A_0) deserve special attention as they are the only modes that exist over the entire frequency spectrum and they carry more energy and have lower attenuation than the higher-order modes. In an active guided wave SHM system, Lamb waves are generated and detected by actuator-sensors, e.g. PZTs [6]. Then a localization method such as imaging methods is used to investigate the integrity of the structure and to find possible crack positions.

Imaging methods for Lamb waves (as a category of localization methods) can be assigned into two general categories, methods based on a baseline signal and beseline-free methods such as time-reversal [11]. In the baseline methods [17] a differential signal is obtained from comparison with the baseline signal from an undamaged structure. To calculate the group velocity, the time of flight of directly propagating waves from each transducer pairs are obtained from the envelope-detected signals [13]. Also differential signals, are calculated by scaling the maximum amplitude of the signal, reduced by the square root of the propagation distance as in [13] to obtain the envelope-detected residual signal $R_{ij}(t)$ from the Hilbert transform as:

$$R_{ij}(t) = \widehat{S}_{ij}(t) - \widehat{S}^{b}_{ij}(t) \tag{1}$$

$$E_{ij}(t) = abs\big(Hilbert\big(R_{ij}(t)\big)\big) \tag{2}$$

where $\widehat{S}_{ij}(t)$ and $\widehat{S}^{b}_{ij}(t)$ are the scaled measured and baseline signals, respectively. $R_{ij}(t)$ is the residual signal and $E_{ij}(t)$ is the envelope-detected residual signal. $E_{ij}(t)$ is the input to both the DAS and SR algorithms described below.

2.2. Delay and Sum method

To perform the DAS method, the signal arrival times for each pixel and each sensor-actuator pair are calculated based on a knowledge of the group velocity. To generate an image of the structure, we have used the method presented in [13] to calculate $P(x,y)$ which is the value of pixel (x,y) in the DAS images:

$$P(x,y) = \frac{1}{N(N-1)} \sum_{i=1}^{N-1} \sum_{j=i+1}^{N} E_{ij}\big(t_{ij}(x,y)\big) \tag{3}$$

where N is the number of transducers and $t_{ij}(x,y)$ is the time-of-flight for a signal that is actuated by PZT "i", scattered at location (x,y) and detected by PZT "j".

2.3. The sparse reconstruction method

The Sparse Reconstruction method is a dictionary-based method based on the assumption of damage sparsity of structures [20]. In this method, it is assumed that the differential signal is composed of a linear combination of signals from individuals scattering points [28]. The residual signals are decomposed into the sparse location-based components that can be analytically computed from the single mode Lamb wave propagation model as follows [20]

$$y(t) = F^{-1}\left\{ \left(\frac{d}{d_{ref}}\right)^{-1/2} F\{x(t)\} exp\left(\frac{-i2\pi fd}{c_p(f)}\right) \right\} \tag{4}$$

where $y(t)$ shows the amplitude of time history of the propagating Lamb wave with excitation time function $x(t)$ after propagating distance d, $F\{\}$ is the Fourier transform operator and $c_p(f)$ is the phase velocity. Also, f is the time frequency.

In the approach of [20], the dictionary matrix $\boldsymbol{A} \in R^{N\times M}$ is formed from these pre-computed signals, and the measurement vector $\mathbf{y} \in R^N$ is formed from the concatenation of differential signals recorded from the structure. By considering a dictionary matrix $\boldsymbol{A}$, a measurement vector $\mathbf{y}$ and using the sparsity assumption, it is possible to reconstruct a sparse vector $\mathbf{x} \in R^M$ which shows the possible location of damage such that

$$\mathbf{y} = \boldsymbol{A}\mathbf{x} + \boldsymbol{e} \tag{5}$$

where $\boldsymbol{e}$ is a noise term. This linear equation is underdetermined if $N < M$ and overdetermined if $N > M$. In the present study, to solve such linear inverse problems, the l_1 optimization method and the well known Basis Pursuit Denoising method (BPDN) are used. The l_1 optimization methods use a linear program to minimize an objective function that

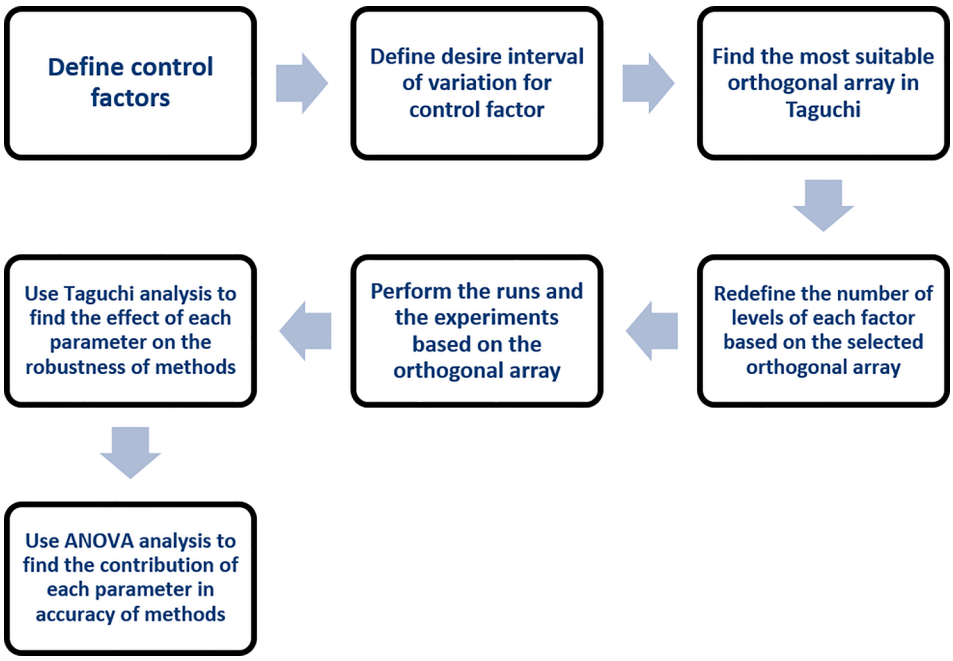

Fig. 1. Proposed evaluation methodology steps.

includes an $l_1$norm term [28]. The BPDN method solves an optimization problem of the form

$$\mathbf{x} = argmin\|\mathrm{x}\|_1 \ subject\ to\ \|\mathbf{y} - \mathbf{A}\mathbf{x}\|_2 \leq \sigma \tag{6}$$

where $\|\ \|_1$ is the $l_1$norm and $\|\ \|_2$ is the $l_2$norm of the vector. Also, σ is the user-specified parameter that should be between $0 \leq \sigma < \|\mathbf{y}\|_2$. Choosing an optimal σ is not straightforward and is a trade off between sparsity (when σ approaches to 1) and reconstruction fidelity (when σ goes to 0). Based the selection of σ on previous works [202528] in this work, we set this value as a random variable in the range $0.6 \leq \frac{\sigma}{\|\mathbf{y}\|_2} < 1$ and considered this variable as an uncontrolled (noise) factor in the Taguchi analysis. Also, to perform the above optimization problem, the free and open-source SPGL1 software package (Version 1.9) was used.

3. Methodology

To perform a reliable assessment of the accuracy and robustness of the DAS and SR methods with a few numbers of statistical data, here the Taguchi method is used as a robust design method for Design of Experiments (DoE).

Furthermore, to study the effects of each individual factor, Taguchi and ANOVA methods are used. Also, to ease in the comparison of different condition results, a metric parameter is designed. Fig. 1 shows the steps of the evaluation methodology proposed in this work.

3.1. Taguchi and ANOVA methods

The Taguchi method is a statistical method developed by Taguchi and Shozo [43]. It was originally used for quality engineering, but nowadays its main application is for studying variation [44] and in Design of Experiments (DoE).

In a problem with several variable factors with several levels, to study the effects of all factors and the effect of all interactions between these factors on the response, the common design of experiments method is the Full-Factorial design [44]. In the Full-Factorial method, the experimental design considers all possible combinations of all the levels across all such factors, which requires a large number of runs to be accomplished. To reduce the number of runs, a well-known method that generates the most information is known as a partial fractional design. However, there are no general guidelines for this method's application or the analysis of the results obtained by performing the experiments [44]. Considering these difficulties, Taguchi formulated a special set of general design guidelines for factorial experiments that cover many applications. Taguchi proposed a design method, which uses an orthogonal array to study all of the parameter space with a lesser number of experiments to be conducted [43]. To use the Taguchi design method, first the main function and the control factors, as well as their levels, must be identified. Then, a suitable orthogonal array is selected and the matrix is constructed. It should be noted that the Taguchi method proposed specific orthogonal arrays and based of the most suitable one, we should redefine the number of levels to be consistent with the that orthogonal array. Finally, the matrix of runs is accomplished, the data is analyzed, and the effect of each factor on the accuracy of each SHM method will be studied. To evaluate the effect of each selected factor, it is necessary to calculate the signal-to-noise ratio (S/N ratio) for each control factor. The S/N ratio in the Taguchi analysis is calculated by the Mean Squared Deviation (MSD) [45] and shows the dependency of the results to controlled and uncontrolled factors (noise factors). A higher value of the S/N shows a low dependency of the results to uncontrolled factors and a higher robustness. To calculate the S/N ratio, the Performance-Index of each image is chosen as the main function and the objective function is considered as the "larger-the-better". The S/N ratio and the mean value for this function is calculated as [44]

$$\eta = \underset{mean=\frac{\sum_{i=1}^{n} Y_i}{n}}{-10\log_{10}\left(\frac{1}{n}\sum_{i=1}^{n}\left(\frac{1}{Y_i}\right)^2\right)} \tag{7}$$

where n is the sample size and Y_i is the target variable.

Then the data will be analysed using ANOVA to test general rather than specific differences among group means in a sample [46]. Also, an ANOVA analysis can determine how likely the changes in results are due to a change in each parameter rather than by chance. This probability is calculated as a p-value that is a probability that measures the evidence against the null hypothesis. Lower probabilities provide stronger evidence against the null hypothesis. The p-value is calculated from an F-value that is the test statistic used to determine whether the term is

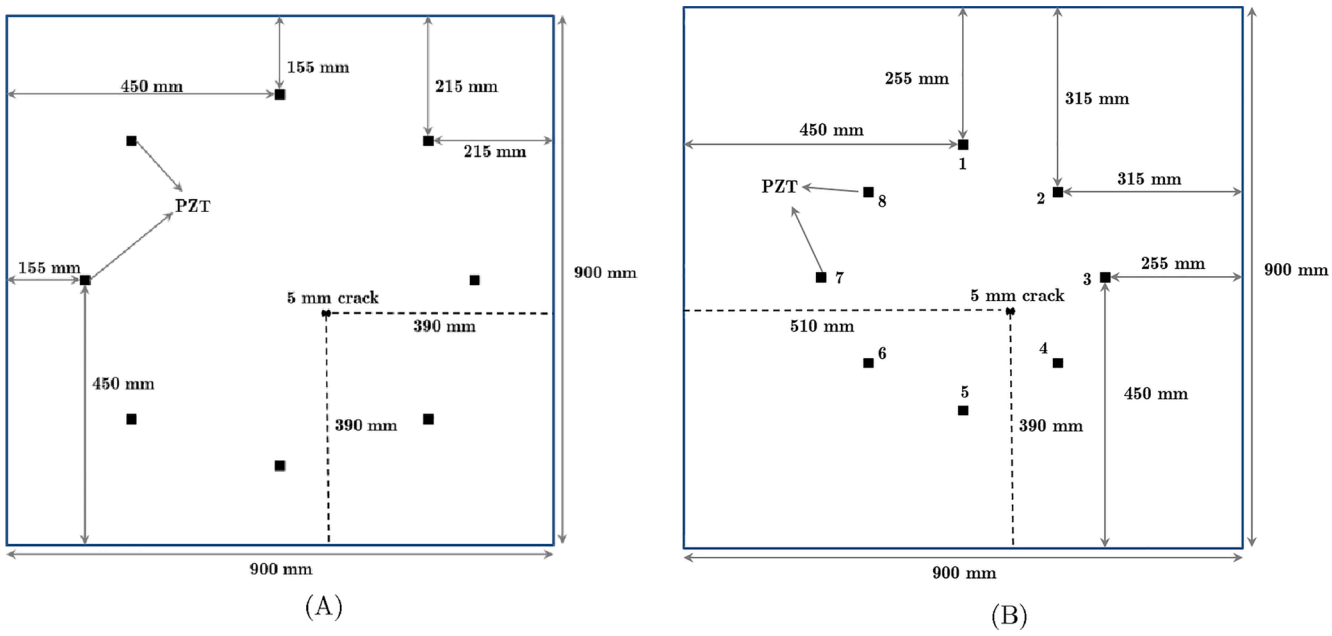

Fig. 2. Two different configurations A and B [25] for PZTs placement.

associated with the response and the F-value is calculated as $\frac{Adj\ MS\ Term}{Adj\ MS\ Error}$ for a 95% level of confidence [44].

3.2. Multi-parameter analysis

To compare the performance of the SR and DAS methods in simulated operational conditions, six parameters with different levels which are considered to influence the SHM system performance were selected. Generally, a larger number of considered levels would result in a better general conclusion, however, the computational cost and time should be in a reasonable range. Based on the number of parameters and the selected Taguchi method requierments, the most suitable orthogonal array was selected as $L_{32}(2^1\ \ 4^5)$, which is combination of 5 parameters in 4 levels and one in 2 levels. The studied conditions are

I. **Poor baseline subtraction due to the temperature changes:** In this work, the temperature is changed in the range 36 °C to 60 °C. 36 °C is the maximum temperature for aluminum in which the Young modulus is considered to be equal to the room temperature modulus [47] and 60 °C is selected according to the highest environmental operatinal temperature for aircraft in Europe based on MIL-STD 180G [48]. The baseline signals are simulated at 36 °C and based on the selcted orthogonal array ($L_{32}(2^1\ \ 4^5)$), the signals from the damaged structure are simulated at 4 points namely 36 °C, 43 °C, 50 °C and 60 °C.

II. **Unwanted signal noise:** In real conditions, the environmental conditions affect the quality of the signals by creating noise, and this makes challenges for damage detection methods. In this work, to assess the robustness of the methods, different levels of white-noise are applied to the residual signals (20 dB, 10 dB, 6 dB, and 3 dB SNR).

III. **Errors in the calculation of wave propagation speed:** In this paper, the traveling wave velocity is calculated as described in Section 2. In this process, some errors could happen due to errors in modeling the wave velocity, errors in the measurement of Time-of-Flight for direct waves, and variation in wave velocity due to inhomogeneity in the material. Therefore, to evaluate the robustness of the two SHM methods, the Lamb waves are modeled with 0%, 1%, 2%, and 3% errors in wave velocity. It should be noted that this error is totally different from the difference between the wave velocities in the baseline signal and measured signal that could happen due to the temperature variation or other operational conditions.

IV. **Model mismatch due to errors in sensor placement:** The exact position of PZTs in real structures may be positioned differently from those in the mathematical model due to measurement errors. In this work, to study the effect of this type of model mismatch, the maximum sensor placement error for each PZT is considered to be 5 mm in any direction on the surface of the plate. The overall error in sensor placement is simulated in four levels SP=(0.0, 1.0, 1.5, 2.0), where $SP = \frac{\sum_{i=1}^{n_p} ds_i}{d_{sp}}$, n_p is the number of PZTs, ds_i is the distance between the exact position of the i^{th} sensor and its position in the mathematical model and d_{sp} is a reference distance equal to the length/width of the PZTs (i.e. 10 mm).

V. **Number of PZTs:** Another parameter that affects the accuracy is the number of sensors and actuators in the SHM system. However, some previous works have focused on the optimal sensor placement which look for the minimization of the uncertainty or maximization of the information gain [49–51], in practice, it seems that using more sensors-actuators should increase accuracy and robustness of the results. However, this also increases experimental and computational costs. In addition, sometimes due to some operational conditions, one or more PZTs may be damaged and disconnected during system operation and it is important for SHM methods to be robust against these conditions. Here, different numbers of sensors-actuators; 8, 7, 6, and 5 PZTs, are considered in the same configuration for damage detection in the plate.

VI. **The effect of boundary reflection:** The reflection of signals from boundaries can cause overlapping signals in the time domain which then cause poor baseline subtraction. In a structure with a uniform boundary condition at all boundaries, the effect of boundary reflection depends on the distance of the actuators from the boundaries. In this work, two configurations, A and B are considered as shown in Fig. 2. In configuration A, the minimum distance of PZTs from the boundary is 155 mm, and the distance of the furthest PZT from the boundary is 215 mm. These two distances for configuration B are 255 mm and 315 mm,

Table 1
Control parameters and their levels.

Parameters (Control Factors)	Levels of Parameter				Noise Factors
	1	2	3	4	
Temperature Variation, A	0 °C	7 °C	14 °C	24 °C	Errors in computational procedures and in determining σ
Signal to noise ratio, B (dB)	3 dB	6 dB	10 dB	20 dB	
Wave propagation speed error, C (%)	0%	1%	2%	3%	Errors due to FEM modeling and material inhomogenity
Sensor placement error, D	0	1	1.5	2	Errors due to other types of model mismatch
Number of sensor-actuators, E	5	6	7	8	
Configuration, F	A		B		

respectively. With respect to selected orthogonal array and because of computational limitations and the good controllability of this parameter, two levels, which have a significant difference in boundary reflection, are considered. In addition, to isolate the effect of boundary reflection, the locations of PZTs are considered in the same pattern in both configurations.

3.3. Test matrix

To use the Taguchi design method, the main function, the control factors, their levels and some noise factors (factors that are uncontrollable) are required. These are summarized in Table 1.

The detail of the matrix of runs accomplished is shown in Table 3 in Section 5.

To determine the accuracy of the reconstructed images, a performance metric parameter is needed. The literature describes different performance metrics, such as the "peak-to-artifact ratio" [20], the exponential coefficient [10] and the absolute error of localization [1933]. Here, it is required to consider more aspects that assess image quality, so a modified performance index (PI) metric is defined that is the combination of previous metrics and some new terms.

$$Performance\ \ Index = \left(\frac{N_{p_i}}{N_{p_t}}\right) \times \sqrt{\left(\frac{d_{cr}}{\Delta d + d_{cr}}\right) \times (\mathrm{PAR}) \times \frac{V_{NP}}{V_{MP}}} \tag{8}$$

In Eq. (8) Δd is the the absolute error of localization [19,33] that has become dimensionless by dividing by the length of the crack d_{cr}. Also, N_{pt} is the total umber of peaks and N_{pi} is the number of peaks in the vicinity of a crack within a radius of 4 cm. In this problem, peaks p_i are defined as every pixel with a value of at least 80% of the maximum pixel value, V_{NP} is the amplitude of the nearest peak to the crack and V_{MP} is the amplitude of maximum peak. Also, *PAR* is the "peak-to-artifact ratio", a performance metric that was introduced by Levine and Michaels [20].

4. Numerical model and experimental setup

In order to compare the accuracy and robustness of the Delay and Sum and SR methods, parameters with different levels were modeled using a commercial FEM software (Ansys Workbench 18.2) using the Explicit Dynamic Solver. The modeled structure was a 90 cm by 90 cm aluminum plate with 3 mm thickness, instrumented with a sparse array of piezo sensor-actuators, to detect and localize a 5 mm horizontal cut-damage with 3 mm depth. To generate the mesh, the solid element and mapped face approach is used. The square PZT actuator-sensors were modelled as an homogeneous material with material properties equal to APC 850, with a length/width of 10 mm and a thickness of 0.3 mm, as well as an infinitesimally small bounding layer. The element size in the worst case is less than 1/17 of the wavelength, and near the crack, it is much smaller (less than 1/100 wavelength). A mesh study was performed, and a proper mesh size was selected. In Fig. 3, an example finite element model mesh of the plate with embedded PZTs and the simulated

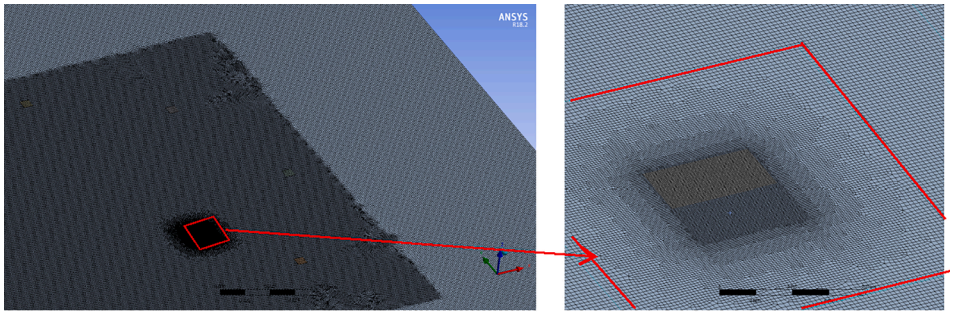

Fig. 3. Finite element model of the plate (a) general overview (b) in the vicinity of the crack.

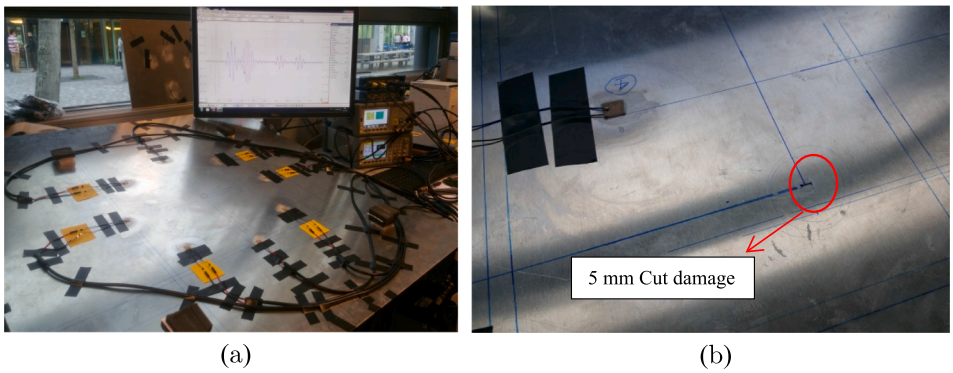

Fig. 4. Experimental setup(a) general setup for data gathering (b) the plate with the cut damage.

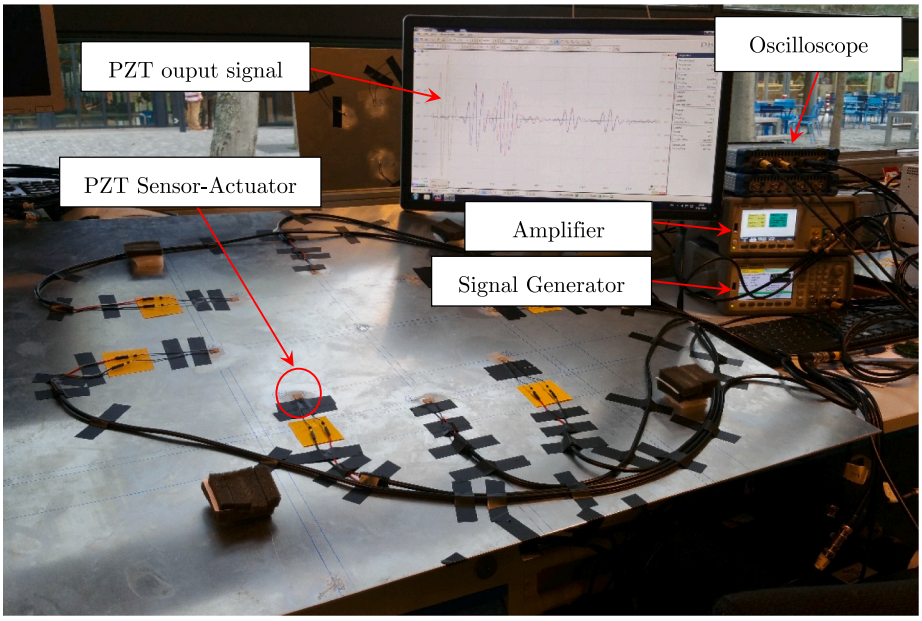

Fig. 5. Experimental equipment used for wave generation and capturing data.

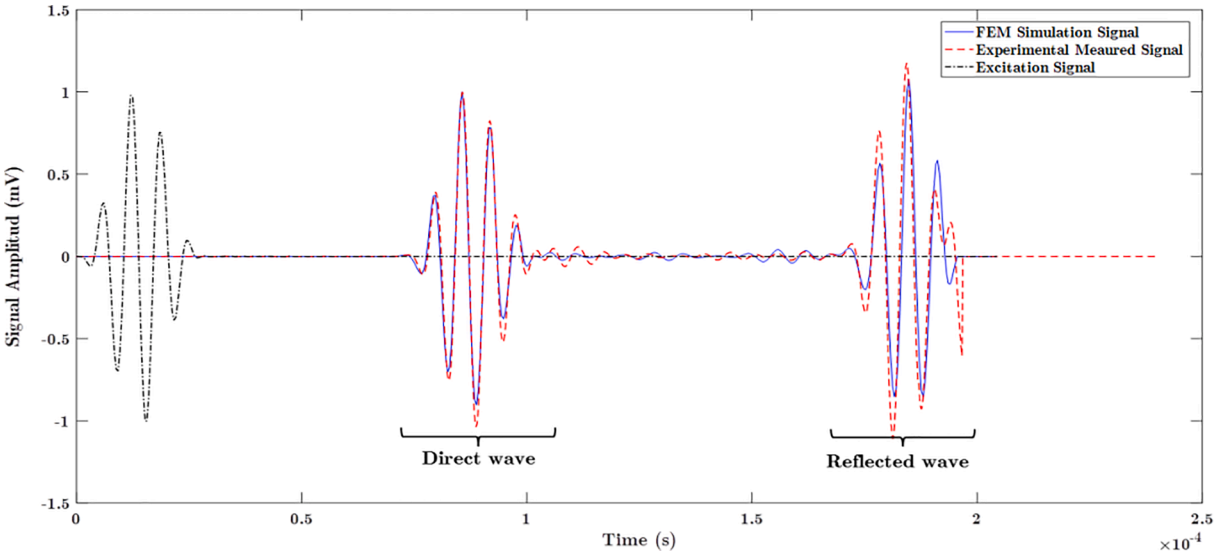

Fig. 6. Comparison between experimental measured and FEM simulated normalized signals.

crack is shown.

To validate the numerical results, experimental testing was performed on the aluminum plate with the same configuration as the "B" configuration in the analytical model, with a through thickness cut of 5 mm cut damage throughout the plate thickness with the width of 0.7 mm at the same position as in the analytical model. The experimental setup is shown in Fig. 4.

Excitation signals were generated by an Agilent 33500B waveform generator and amplified by an Agilent 33502A wideband voltage amplifier. PZT signals were captured using a PicoScope 6402 oscilliscope, connected using cables with BNC connectors. The mentioned equipment is shown in Fig. 5.

In both the numerical analysis and the experimental test, for the Lamb wave generation, a 150 kHz four-cycle Hann windowed tone burst was used as an excitation signal. Each transducer acts in turn as a wave generator while all the other transducers capture signals. Also, we have used two PZT were positioned on opposite sides of the plate, to excite the plate with the pure S0 Lamb-wave mode.

5. Results

In this section, experiment and numerical results are first compared to verify the numerical results. After verification, the numerical results are processed using both the DAS and SR methods. It should be noted that as the type of images reconstructed from these two methods is different, so it is not possible to directly compare the images from the two methods. However, it is possible to compare the trends in the processed data when the control parameters are changed. For this purpose, the Taguchi and ANOVA analyses are used for the comparison of the DAS and SR results.

5.1. Comparison of experimental and numerical results

In this section, the ultrasonic wave signals from the numerical

Table 2
Comparison of normalized calculated PI using experimental and simulation data.

	Normalized PI (Experimental)		Normalized PI (Simulation)	
Run Number	DAS	SR	DAS	SR
5	**80**	**100**	**83**	**100**
6	**100**	**48**	**100**	**51**
7	**32**	**1**	**28**	**1**
8	**58**	**20**	**88**	**14**

simulations are compared with those from experimental testing to verify the numerical simulations. In Fig. 6, the numerical and experimental signals due to pure S0 Lamb waves propagated by PZT 1 and received by PZT 5 are depicted (the position of the PZTs is shown in Fig. 2(B)). The excitation signal that shown in Fig. 6 is normalized to its maximum value and the received signals are normalized with respect to maximum peak of the direct waves.

As it can be seen in Fig. 6, there is a good agreement between experimental and simulated signals for the direct wave. However, there is some difference in the peak values of the signals that is due to a difference in the sampling frequency of the two signals as some data points are not measured in the FEM simulated signal. In addition, because of

Table 3
Normalized calculated PI for numerically modelled data using SR and DAS Method.

	Control Factors						Normalized PI		
Run Number	A(°C)	B (dB)	C (%)	D	E	F	DAS	SR	Difference
1	0	20	0	0.0	8	B	**100**	**100**	**0**
2	0	10	1	1.0	7	B	**100**	**74**	**26**
3	0	6	2	1.5	6	B	**100**	**54**	**46**
4	0	3	3	2.0	5	B	**63**	**43**	**20**
5	7	20	0	1.0	7	B	**69**	**100**	**−31**
6	7	10	1	0.0	8	B	**83**	**51**	**32**
7	7	6	2	2.0	5	B	**23**	**1**	**22**
8	7	3	3	1.5	6	B	**73**	**14**	**59**
9	14	20	1	1.5	5	B	**8**	**1**	**7**
10	14	10	0	2.0	6	B	**53**	**60**	**−7**
11	14	6	3	0.0	7	B	**52**	**44**	**8**
12	14	3	2	1.0	8	B	**66**	**1**	**65**
13	24	20	1	2.0	6	B	**19**	**41**	**−22**
14	24	10	0	1.5	5	B	**1**	**1**	**0**
15	24	6	3	1.0	8	B	**13**	**12**	**1**
16	24	3	2	0.0	7	B	**34**	**44**	**−10**
17	0	20	3	0.0	5	A	**55**	**89**	**−34**
18	0	10	2	1.0	6	A	**100**	**27**	**73**
19	0	6	1	1.5	7	A	**99**	**82**	**17**
20	0	3	0	2.0	8	A	**70**	**75**	**−5**
21	7	20	3	1.0	6	A	**9**	**9**	**0**
22	7	10	2	0.0	5	A	**11**	**28**	**−17**
23	7	6	1	2.0	8	A	**24**	**94**	**−70**
24	7	3	0	1.5	7	A	**10**	**1**	**9**
25	14	20	2	1.5	8	A	**17**	**1**	**16**
26	14	10	3	2.0	7	A	**8**	**1**	**7**
27	14	6	0	0.0	6	A	**21**	**1**	**20**
28	14	3	1	1.0	5	A	**14**	**1**	**13**
29	24	20	2	2.0	7	A	**1**	**1**	**0**
30	24	10	3	1.5	8	A	**1**	**1**	**0**
31	24	6	0	1.0	5	A	**7**	**1**	**6**
32	24	3	1	0.0	6	A	**4**	**47**	**−43**
Average							**40.9**	**34.4**	

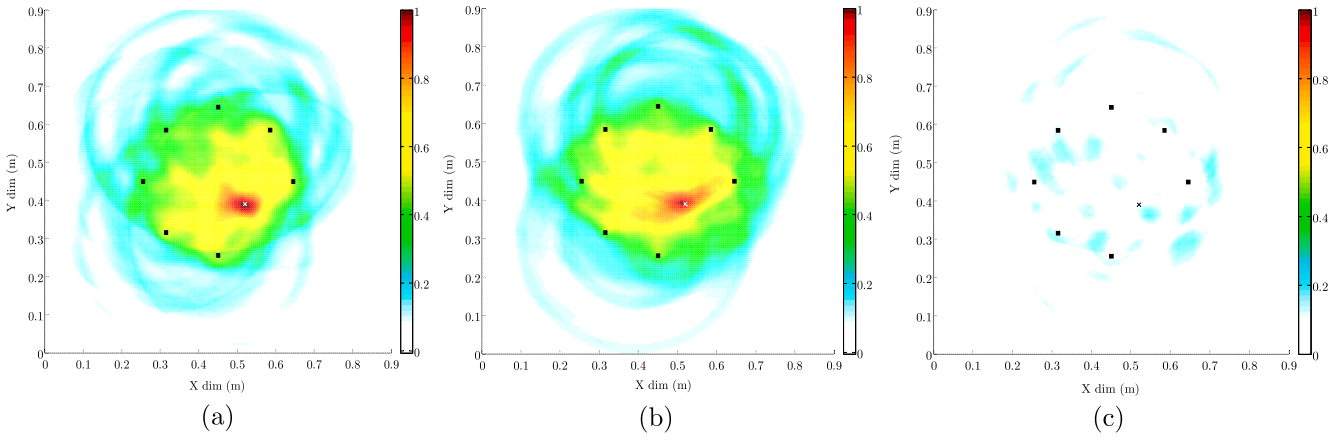

Fig. 7. Comparison of images for configuration B, run 5 constructed using DAS via (a) experimental measured signals (b) FEM simulated signals (c) difference between experimental and FEM results. "×" is the experimental defect location and black squres are the sesnsor locations.

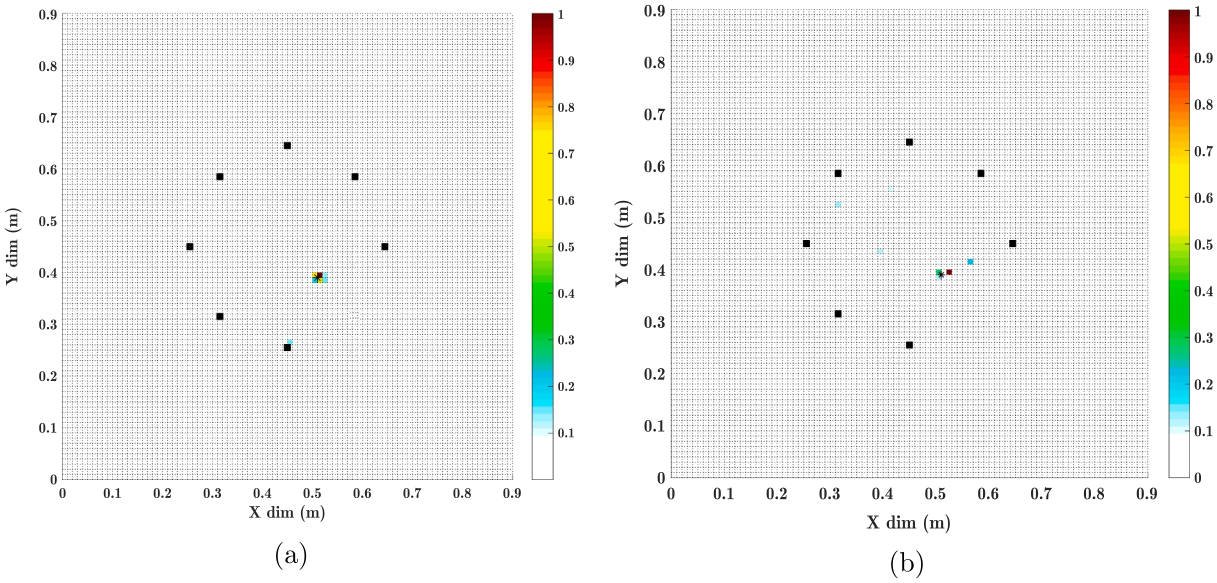

Fig. 8. Comparison of images constructed using SR via (a) experimentally measured signals (b) FEM simulated signals. "×" is the experimental defect location and black squres are the sesnsor locations.

complexity in boundary reflection and mode conversion phenomena, some differences can be seen between reflected waves in experimental and simulated signals. As a quantitive comparison, the difference between the RMS of two signals is about 1% and the cosine similarity between these two signals is about 0.9. In Table 2, a comparison is performed between the normalized calculated PI from the experimental and the simulation data using DAS and SR methods in the four different conditions (run numbers 5 to 8 in Table 3).

As can be seen from Table 2, the experimental and simulation results are in good agreement. However, there are some differences that could be due to not-ideally isolated parameters in the experimental condition. Figs. 7 and 6 show images constructed using DAS and SR methods via experimental and simulation data, respectively. These images are constructed in the condition that was introduced in run 5 of Table 2.

As it can be seen in Fig. 7(c) and from contour bar, the maximum difference between images reconstructed via simulated and experimental data is about 25% of the maximum value of the contour which shown in Fig. 7(a) and (b).

The images presented in Fig. 8 shows the predicted damage location in images reconstructed using simulated data agree with ones using experimental data within about 1 pixel. The results presented in Fig. 6 as well as in Table 2 shows the verification of simulation data that will be analyzed in the next step.

5.2. Conducting the matrix of runs

Here regarding $L_{32}(2^1 \quad 4^5)$ presented in Table 3, numerical simulations were performed according to the factors and levels are shown in Table 1. The normalized PI was calculated for each run and each method and are presented in Table 3. Also, a min/max normalization was performed on the PIs for each method, and the normalized data were scaled between 1 and 100.

As is shown in Table 3, the change of PI in the DAS method is smoother than the SR method. In the results from the SR method, one can see that in some cases, the result suddenly falls to one.

It sould be noted that in this study a simple structure was considered as a test case because it was important that the modelled structure was both simple enough to model the Lamb wave propagation accurately and to reduce the uncontrolled factors as least as possible, and also of a suitable size that it was computationally manageable to perform the FE-analysis. In addition, in real engineering complex structures, it is very difficult to study the effect of "boundary reflection" parameter because the multipath reflections are very complicated and dependent to other factors.

In Complex structures, the effect of model mismatch seems much more serious than simple structures, because due to the existence of multipath reflections, modeling the propagation of Lamb waves is more challenging than simple structures. For example, to calculate wave velocity, it is very difficult to find the exact time-of-flight for direct waves in complex structures due to the interference of reflective waves with direct waves. Also, the poor baseline subtraction in complex structures is more than simple structures due to the repetition of subtraction errors in reflection waves. However, the comparison of DAS and SR methods in simple and complex structures does not seem to be much different from each other.

5.3. Constructed images

In this section, sample images with various PIs constructed using simulated data from specific runs are depicted in Figs. 9 and 10 to demonstrate the consistency of image quality and PI number.

As is shown in Fig. 9 in the DAS method, decreasing the PI index the spot size become larger and obscures the exact location of damage and in the case with the very small PI the spot area shows the wrong location of the defect. Also, by decreasing the PI index in images reconstructed via SR method depicted in Fig. 10, false detection increases and in case of very small PIs the detection totally failed.

5.4. Taguchi analysis result

In this section, after performing the runs presented in Table 3, to evaluate the effect of each factor on the quality and robustness of results, the mean values and the S/N ratio for each control factor are calculated. In the Taguchi analysis the S/N shows the dependency of the results to control and noise factors and a higher value of the S/N shows a low dependency of the results to noise factors and a higher robustness. The average of S/N is shown in Table 4 and the mean values of PIs for each level of control factor are presented in Table 5. Also, in these tables the "Delta" shows the difference between the maximum and minimum values and the "Rank" shows the ranking of each parameter with respect to higher value of Delta.

According to Table 4, it can be seen that the overall robustness of the

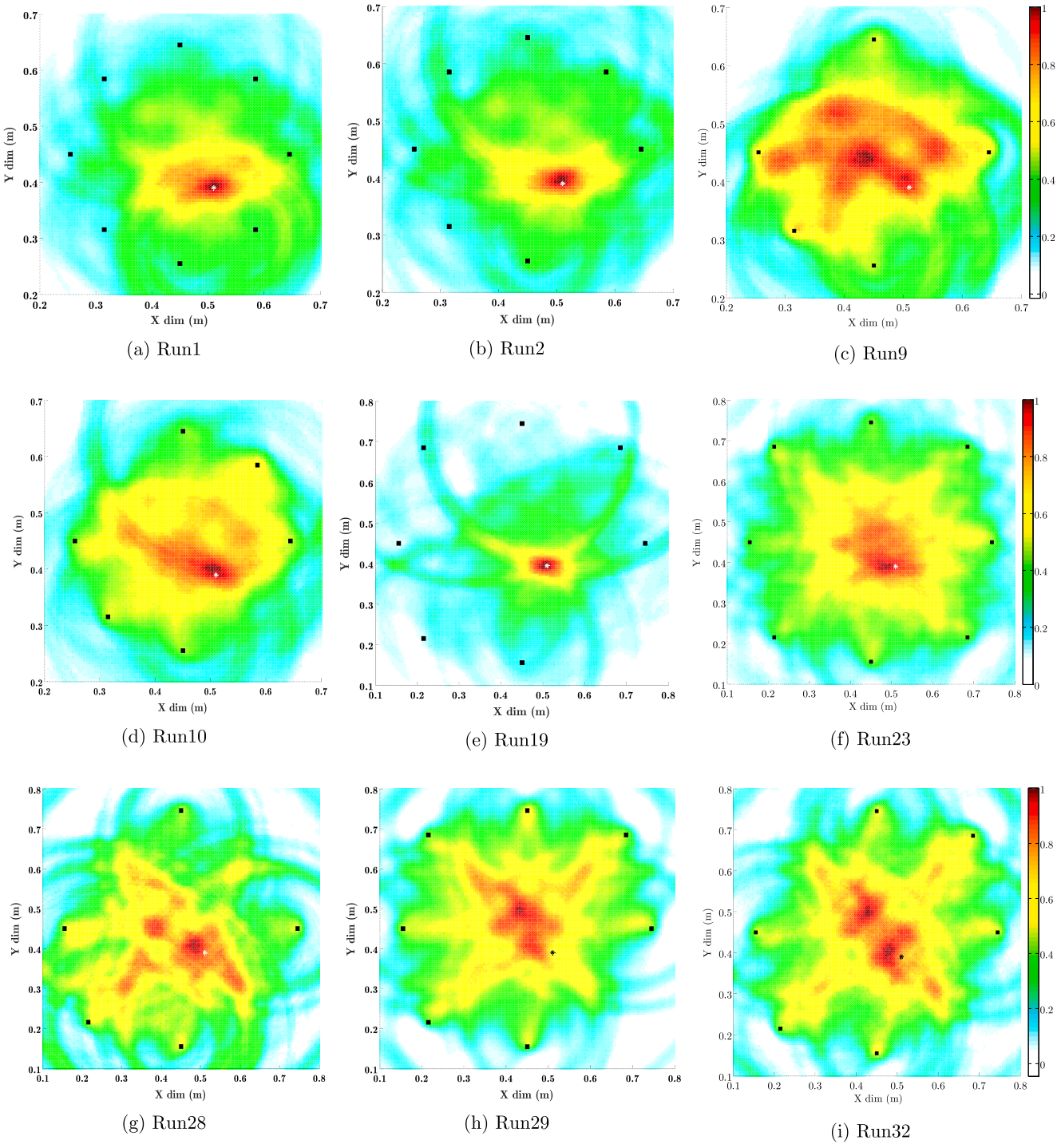

Fig. 9. Images constructed using simulated data via DAS. "×" denotes defect location and black squres are the sensor locations.

DAS method against noise factors is better than the SR method. This seems logical because of the complexity of the calculations of the SR method against the simplicity of the DAS method.

As we would expect from literature [13,19], the accuracy and robustness of the methods are very sensitive to temperature changes and the best accuracy and robustness is achieved when no temperature change occurs. Beyond that the DAS and SR methods show different sensitivities to the varing parameters. The DAS method is more sensitive to a change in boundary reflection and to a lesser extent the number of PZTs. But in the SR method, the effect of temperature changes and boundary reflection on the accuracy of results are less than those in the DAS method. Also, in the SR method, one can find more significant changes in results due to change in the Signal-to-Noise ratio (SNR) of data, error in wave speed calculation and error in sensor placement rather than DAS method. The results of Tables 4 and 5 are depicted in graphs in Figs. 11 and 12.

According to graphs depicted in Figs. 11 and 12, it can be concluded that

- The robustness and accuracy of the SR method falls down when the temperature changes from 7 °C to 14 °C, but the robustness of the DAS method does not change significantly in this range. Also, about

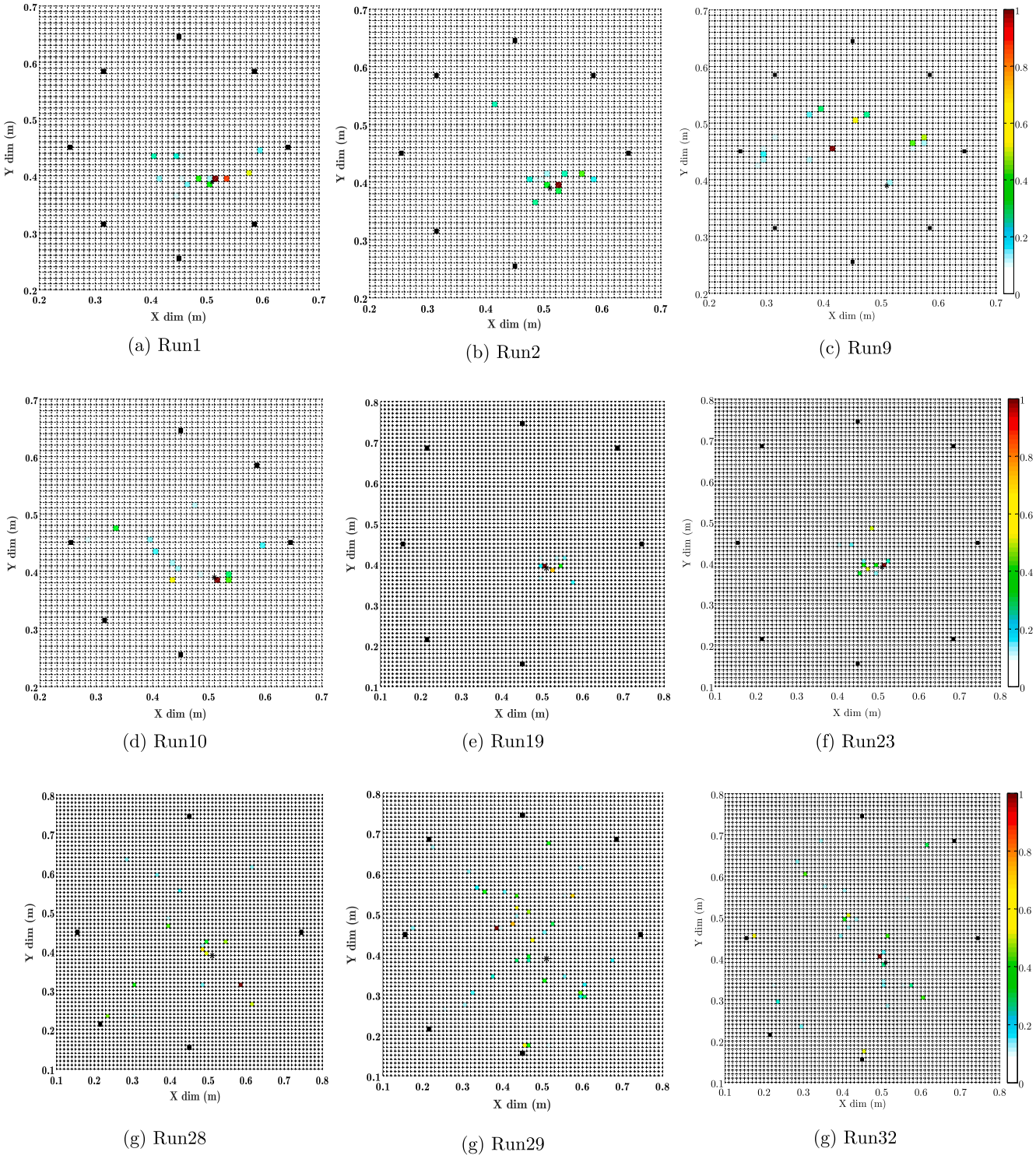

Fig. 10. Images constructed using simulated data via SR. "×" denotes defect location and black squres are the sesnsor locations.

the boundary reflection effect, the results show that a greater distance of sensor-actuators from the boundary leads to better results in both methods.

- About the error in wave speed calculation, the best result is achieved for 1% error. It should be noted that, in the developed code, the wave speed is calculated from direct waves traveling between sensors and actuators and this calculation may have some computational errors. Thus it is also possible for the calculated speed with 1% change to be closer to the true wave speed.

About the number of PZTs, in the SR method, the accuracy of the method reduces when the number of PZTs reduces from 7 to 6. But, there is not a significant difference in the results of 7 and 8 PZTs. In the DAS results this behavior happens when the number of PZTs changes from 5 to 6. It seems that in both methods, if the number of sensors exceeds a certain number, the accuracy of damage location will not change vs. number of PZTs and the slope of the curve (mean of accuracy vs. number of PZTs) tend to zero after that certain number. This means that for a specific network geometry there is an optimal number of PZTs that using

Table 4
Response table for the S/N ratio for the DAS and SR methods.

Level	Boundary reflection		Temperature change (°C)		Signal to Noise (dB)		Error in Wave Speed		Error in Sensor Placement		Number of PZTs	
	DAS	SR	DAS	SR	DAS	SR	DAS	SR	DAS	SR	DAS	SR
1	22.5	13.5	38.5	36.0	28.9	16.5	26.4	19.1	29.6	26.5	22.1	13.0
2	31.1	25.6	28.4	21.9	29.3	21.6	27.9	22.8	29.3	16.7	29.3	20.0
3			27.0	8.6	24.0	21.1	27.5	16.1	22.5	12.7	27.5	22.7
4			13.3	11.6	24.9	18.9	25.3	20.1	25.8	22.2	28.2	22.4
Delta	8.6	12.1	25.2	27.5	5.3	5.1	2.6	6.7	7.1	13.8	7.2	9.7
Rank	2	3	1	1	5	6	6	5	4	2	3	4

Table 5
Response table for the means value of PI for the DAS and SR methods.

Level	Boundary reflection		Temperature change(°C)		Signal to Noise (dB)		Error in Wave Speed		Error in Sensor Placement		Number of PZTs	
	DAS	SR	DAS	SR	DAS	SR	DAS	SR	DAS	SR	DAS	SR
1	28.2	26.1	85.9	68.1	41.7	24.2	41.4	42.3	44.9	46.9	22.7	22.3
2	53.5	41.9	37.8	40.1	42.3	37.7	43.7	43.7	47.3	28.6	47.4	26.6
3			29.9	13.8	44.7	32.5	44.1	21.3	38.7	21.1	46.6	43.4
4			9.8	14.1	34.7	41.7	34.4	28.9	32.7	39.5	46.7	43.9
Delta	25.4	15.8	76.1	54.3	10.0	17.5	9.7	22.4	14.6	25.8	24.7	21.6
Rank	2	6	1	1	5	5	6	3	4	2	3	4

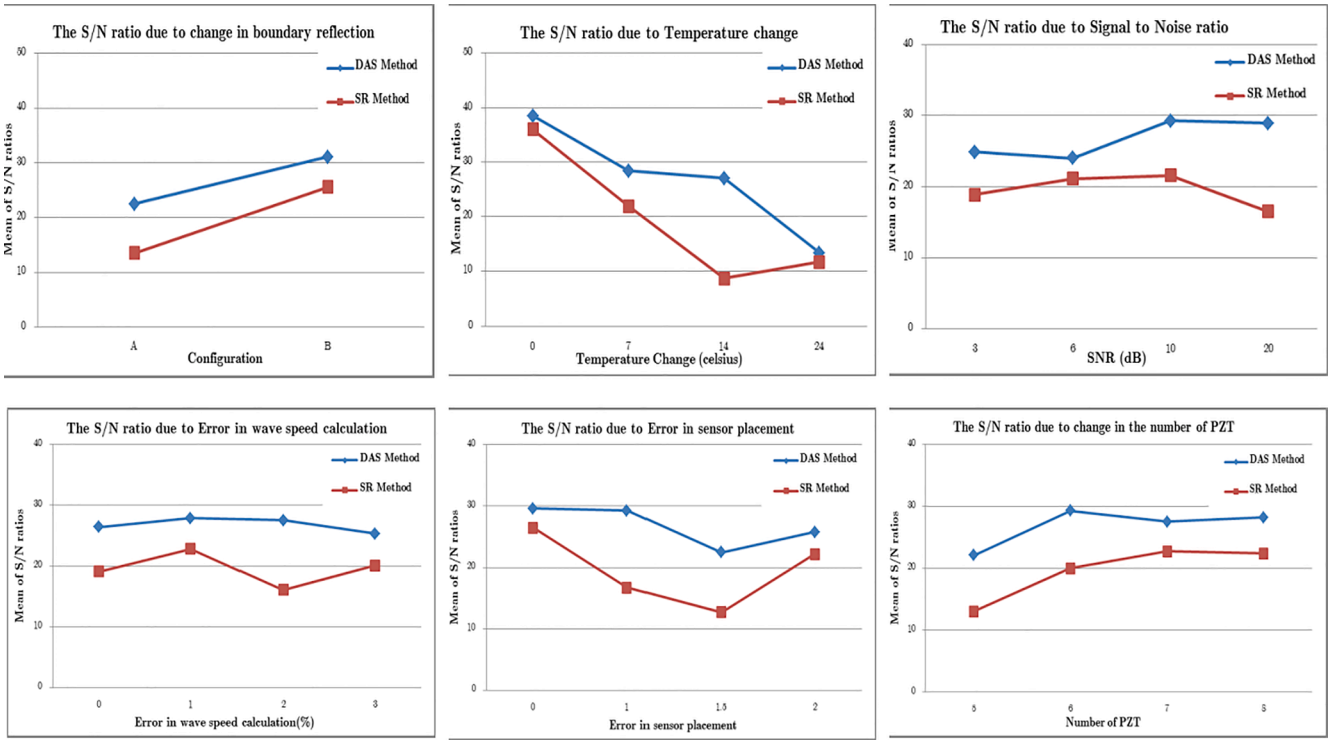

Fig. 11. Main effect plot for S/N ratios for results of the DAS and SR methods.

PZT more than the optimal number does not significantly improve the accuracy of the results. This behavior, which is due to the increased overlap of the wave propagation path and PZT signals in a defined geometry, occurs when the number of PZTs exceeds the optimal number.

5.5. ANOVA analysis result

In this section, an ANOVA analysis is performed to estimate the contribution of each factor on changes in the PIs for each method. Also, ANOVA analysis can determine, how likely the changes in results are due to a change in each parameter rather than by other errors. This probability is calculated as a p value that is a probability that measures the evidence against the null hypothesis. Lower probabilities provide stronger evidence against the null hypothesis. The results of the ANOVA of the PIs are given in Table 6 for the DAS method and in Table 7 for the SR method. In Tables 6 and 7 $(1-p) \times 100$ shows how important are differences seen in Tables 4 and 5. For instance, Table 7 shows that the change of SNR in the defined range does not make significant impact on the results. Also, In Tables 6 and 7 "Seq SS" is the sequential sums of squares measured of variation of PIs, "Adj MS" is the adjusted mean square and "DF" is the total number of degrees of freedom.

As it can be seen from the percentage of contribution column in

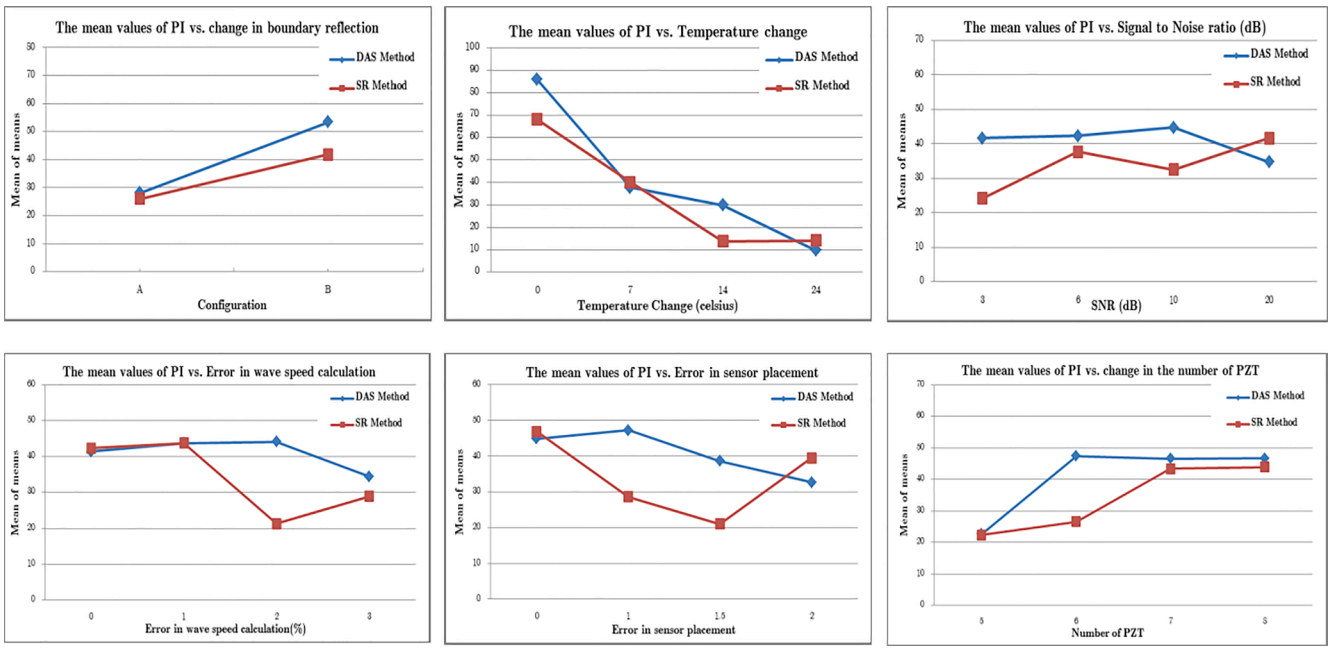

Fig. 12. Main effect plot for means for results of the DAS and SR methods.

Table 6
ANOVA results of the PI calculated from the DAS method.

Source	DF	Seq SS	Adj MS	F-value	p-value	$(1-p)\times 100$	Percentage of contribution
Boundary reflection	1	5149	5149	20.38	0.000	100%	33,10%
Temperature change	3	24,996	8332	32.98	0.000	100%	53,56%
Signal to Noise	3	445	148	0.59	0.633	36.7%	0,95%
Error in Wave Speed	3	484	161	0.64	0.601	39.9%	1,04%
Error in Sensor Placement	3	1033	344	1.36	0.292	70.8%	2,22%
Number of PZT	3	3505	1168	4,63	0,018	98,2%	7,51%
Error	15	3789	252				1,62%
Total	31	39,404	15,557				100%

Table 7
ANOVA results of the PI calculated from the SR method.

Source	DF	Seq SS	Adj MS	F-value	p-value	$(1-p)\times 100$	Percentage of contribution
Boundary reflection	1	1994	1994	3,02	0,103	89,7%	17,4%
Temperature change	3	16,038	5346	8,09	0,002	99,8%	46,5%
Signal to Noise	3	1373	457	0,69	0,571	42,9%	4,0%
Error in Wave Speed	3	2801	933	1,41	0,278	72,2%	8,1%
Error in Sensor Placement	3	3126	1042	1,58	0,237	76,3%	9,1%
Number of PZT	3	3014	1005	1,52	0,250	75%	8,7%
Error	15	9917	661				5,8%
Total	31	38,262	11,439				100%

Table 6, the parameters that most determines the accuracy of the results in the DAS method is the temperature change, with the boundary reflection and number of PZTs in the second and third levels, respectively. The three other parameters have a negligible contribution in the results. Also, it can be noted that the probability of contribution of each parameter, as shown by $(1-p)\times 100$ are in good agreement with the percentage of contribution.

Table 7 shows the percentage of contribution of each parameter in the results of the SR method. The most dominant parameter in the accuracy of the results is again temperature change, and the boundary reflection is the second most dominant parameter. However, the levels of the next three parameters are almost similar to each other. Also, it is noted that the probability of the contribution of each parameter, as shown by $(1-p)\times 100$, is in good agreement with the percentage of contribution.

6. Conclusion

In this paper, for performance assessment of SHM methods, a methodology based on the Taguchi method is proposed. Also, comparisons were performed between two SHM methods, SR and DAS, in a specific limited performance region and on a test case with simple geometry. For this purpose, a performance metric parameter (PI) was defined and six variable conditional parameters were chosen which included temperature-variation, boundary-reflection, SNR, error in sensor placement, error in the calculation of wave-speed and number of PZTs. Also, for the design of test matrix and statistical analysis, the Taguchi and ANOVA methods were used.

Based on the results, it could be concluded that the overall robustness of the DAS method with respect to noise factors is better than the SR method. Also, it can be concluded that the SR method was more robust than the DAS method with respect to changes in boundary reflection and temperature changes (factors that cause poor baseline subtraction). These conclusions show that these two methods could complement each other and that the combination of these two methods could improve the performance of damage localization under the defined conditions. In addition, using the proposed evaluation method for real engineering structures and considering some other operational conditions (such as applying loads and humidity) are interesting and practical ideas for future work.

In conclusion, because of the inherent difference of the pictures that are constructed with these two methods, it is quite difficult to visually compare the accuracy of methods, but it was possible to compare the robustness and behaviour of these two methods using the Taguchi and ANOVA methods as has been demonstrated in this paper. In addition, it should be noted the conclusions presented in this paper, are valid in the defined performance region and to obtain more comprehensive conclusions, a much larger and prohibitively computationally expensive data set would be required.

CRediT authorship contribution statement

A. Nokhbatolfoghahai: Conceptualization, Methodology, Data curation, Software, Writing - original draft. **H.M Navazi:** Supervision, Conceptualization, Methodology, Writing - review & editing. **R.M. Groves:** Supervision, Methodology, Writing - review & editing.

Declaration of Competing Interest

The authors declare that they have no known competing financial interests or personal relationships that could have appeared to influence the work reported in this paper.

References

[1] D. Balageas, C.P. Fritzen, A. Güemes (Eds.), Structural Health Monitoring, vol. 90, John Wiley & Sons, 2010.
[2] V. Giurgiutiu, Structural Health Monitoring with Piezoelectric Wafer Active Sensors, Academic Press, 2014.
[3] H. Lamb, On waves in an elastic plate, Proc. R. Soc. Lond. A 93 (648) (1917) 114–128.
[4] M. Mitra, S. Gopalakrishnan, Guided wave based structural health monitoring: a review, Smart Mater. Struct. 25 (5) (2016), 053001.
[5] P. Ochôa, V. Infante, J.M. Silva, R.M. Groves, Detection of multiple low-energy impact damage in composite plates using Lamb wave techniques, Compos. B Eng. 80 (2015) 291–298.
[6] Z. Su, L. Ye, Identification of damage using Lamb waves: from fundamentals to applications, vol. 48, Springer Science & Business Media, 2009.
[7] P. Malinowski, T. Wandowski, I. Trendafilova, W. Ostachowicz, A phased array-based method for damage detection and localization in thin plates, Struct. Health Monitor. 8 (1) (2009) 5–15.
[8] X. Zhao, R.L. Royer, S.E. Owens, J.L. Rose, Ultrasonic Lamb wave tomography in structural health monitoring, Smart Mater. Struct. 20 (10) (2011), 105002.
[9] B. Alem, A. Abedian, A semi-baseline damage identification approach for complex structures using energy ratio correction technique, Struct. Control Health Monitor. 25 (2) (2018), e2103.
[10] J.S. Hall, J.E. Michaels, Minimum variance ultrasonic imaging applied to an in situ sparse guided wave array, IEEE Trans. Ultrason. Ferroelectr. Freq. Control 57 (10) (2010) 2311–2323.
[11] C.H. Wang, J.T. Rose, F.K. Chang, A synthetic time-reversal imaging method for structural health monitoring, Smart Mater. Struct. 13 (2) (2004) 415.
[12] I. Dafydd, Z. Sharif Khodaei, Analysis of barely visible impact damage severity with ultrasonic guided Lamb waves, Struct. Health Monitor. (2019), 1475921719878850.
[13] J.E. Michaels, Detection, localization and characterization of damage in plates with an in situ array of spatially distributed ultrasonic sensors, Smart Mater. Struct. 17 (3) (2008), 035035.
[14] S. Shan, J. Qiu, C. Zhang, H. Ji, L. Cheng, Multi-damage localization on large complex structures through an extended delay-and-sum based method, Struct. Health Monitor. 15 (1) (2016) 50–64.
[15] T. Stepinski, L. Ambroziński, T. Uhl, Beamforming of Lamb waves using 2D arrays: a comparative study, in: The 9th International Workshop on Structural Health Monitoring, Stanford University, USA, September, 2013.
[16] J.S. Hall, P. Fromme, J.E. Michaels, Ultrasonic guided wave imaging for damage characterization, Aicr. Airworth. Sust. Conf. 2011 (2011) 1–13.
[17] Z. Sharif-Khodaei, M.H. Aliabadi, Assessment of delay-and-sum algorithms for damage detection in aluminium and composite plates, Smart Mater. Struct. 23 (7) (2014), 075007.
[18] M.S. Salmanpour, Z. Sharif Khodaei, M.H. Aliabadi, Transducer placement optimisation scheme for a delay and sum damage detection algorithm, Struct. Control Health Monitor. 24 (4) (2017), e1898.
[19] M. Salmanpour, Z. Sharif Khodaei, M. Aliabadi, Impact damage localisation with piezoelectric sensors under operational and environmental conditions, Sensors 17 (5) (2017) 1178.
[20] R.M. Levine, J.E. Michaels, Model-based imaging of damage with Lamb waves via sparse reconstruction, J. Acoust. Soc. Am. 133 (3) (2013) 1525–1534.
[21] R. Levine, J.E. Michaels, Block-sparse reconstruction and imaging for lamb wave structural health monitoring, IEEE Trans. Ultrason. Ferroelectr. Freq. Control 61 (6) (2014) 1006–1015.
[22] W. Wang, Y. Bao, W. Zhou, H. Li, Sparse representation for Lamb-wave-based damage detection using a dictionary algorithm, Ultrasonics 87 (2018) 48–58.
[23] J. Hua, Z. Wang, F. Gao, L. Zeng, J. Lin, Sparse reconstruction imaging of damage for Lamb wave simultaneous excitation system in composite laminates, Measurement 136 (2019) 201–211.
[24] C.B. Xu, Z.B. Yang, Z. Zhai, B.J. Qiao, S.H. Tian, X.F. Chen, A weighted sparse reconstruction-based ultrasonic guided wave anomaly imaging method for composite laminates, Compos. Struct. 209 (2019) 233–241.
[25] A. Nokhbatolfoghahai, H.M. Navazi, R.M. Groves, Use of delay and sum for sparse reconstruction improvement for structural health monitoring, J. Intell. Mater. Syst. Struct. 30 (18–19) (2019) 2919–2931.
[26] A. Nokhbatolfoghahai, H.M. Navazi, R.M. Groves, Using the hybrid DAS-SR method for damage localization in composite plates, Compos. Struct. (2020), 112420.
[27] A. Golato, S. Santhanam, F. Ahmad, M.G. Amin, Multimodal sparse reconstruction in guided wave imaging of defects in plates, J. Electron. Imaging 25 (4) (2016), 043013.
[28] R.M. Levine, Ultrasonic Guided Wave Imaging Via Sparse Reconstruction, Doctoral dissertation, Georgia Institute of Technology), 2014.
[29] O. Putkis, R.P. Dalton, A.J. Croxford, The influence of temperature variations on ultrasonic guided waves in anisotropic CFRP plates, Ultrasonics 60 (2015) 109–116.
[30] S. Ha, K. Lonkar, A. Mittal, F.K. Chang, Adhesive layer effects on PZT-induced lamb waves at elevated temperatures, Struct. Health Monitor. 9 (3) (2010) 247–256.
[31] Y. Lu, J.E. Michaels, Feature extraction and sensor fusion for ultrasonic structural health monitoring under changing environmental conditions, IEEE Sens. J. 9 (11) (2009) 1462–1471.
[32] G. Aranguren, P.M. Monje, V. Cokonaj, E. Barrera, M. Ruiz, Ultrasonic wave-based structural health monitoring embedded instrument, Rev. Sci. Instrum. 84 (12) (2013), 125106.
[33] L. Qiu, S. Yuan, X. Zhang, Y. Wang, A time reversal focusing based impact imaging method and its evaluation on complex composite structures, Smart Mater. Struct. 20 (10) (2011), 105014.
[34] M.S. Salmanpour, Z. Sharif Khodaei, M.H. Aliabadi, Guided wave temperature correction methods in structural health monitoring, J. Intell. Mater. Syst. Struct. 28 (5) (2017) 604–618.
[35] J. Moriot, N. Quaegebeur, A. Le Duff, P. Masson, A model-based approach for statistical assessment of detection and localization performance of guided wave–based imaging techniques, Struct. Health Monitor. 17 (6) (2018) 1460–1472.
[36] J.E. Michaels, Sparse array imaging with guided waves under variable environmental conditions, in: Structural Health Monitoring (SHM) in Aerospace Structures, Woodhead Publishing, 2016, pp. 255–284.
[37] Y. Ren, L. Qiu, S. Yuan, F. Fang, Gaussian mixture model and delay-and-sum based 4D imaging of damage in aircraft composite structures under time-varying conditions, Mech. Syst. Sig. Process. 135 (2020), 106390.
[38] A.J. Croxford, J. Moll, P.D. Wilcox, J.E. Michaels, Efficient temperature compensation strategies for guided wave structural health monitoring, Ultrasonics 50 (4–5) (2010) 517–528.
[39] Z. Zhang, Y. Zhong, J. Xiang, Y. Jiang, Phase correction improved multiple signal classification for impact source localization under varying temperature conditions, Measurement 152 (2020), 107374.
[40] C. Fendzi, M. Rebillat, N. Mechbal, M. Guskov, G. Coffignal, A data-driven temperature compensation approach for Structural Health Monitoring using Lamb waves, Struct. Health Monitor. 15 (5) (2016) 525–540.
[41] H. Zhang, J. Hua, F. Gao, J. Lin, Efficient Lamb-wave based damage imaging using multiple sparse Bayesian learning in composite laminates, NDT E Int. (2020), 102277.
[42] M. Zhao, W. Zhou, Y. Huang, H. Li, Sparse Bayesian learning approach for propagation distance recognition and damage localization in plate-like structures using guided waves, Struct. Health Monitor. (2020), 1475921720902277.
[43] G. Taguchi, S. Konishi, Taguchi Methods: Orthogonal Arrays and Linear Graphs: Tools for Quality Engineering, American Supplier Institute, 1987.
[44] R.S. Rao, C.G. Kumar, R.S. Prakasham, P.J. Hobbs, The Taguchi methodology as a statistical tool for biotechnological applications: a critical appraisal, Biotechnol. J.: Healthcare Nutr. Technol. 3 (4) (2008) 510–523.
[45] G. Taguchi, Introduction to quality engineering: designing quality into products and processes (No. 658.562 T3), 1986.
[46] D.M. Lane, Introduction to Statistics: An Interactive e-Book. Available at http://davidmlane.com/hyperstat/, 2013.

[47] R.C. Rice, Metallic Materials Properties Development and Standardization (MMPDS): Chapters 1–4, vol. 1. National Technical Information Service, 2003.
[48] M.K. Thompson, MIL-STD-810G Environmental Engineering Considerations and Laboratory Tests, US Department of Defense, Washington, DC, USA, 2008.
[49] S. Cantero-Chinchilla, J. Chiachío, M. Chiachío, D. Chronopoulos, A. Jones, Optimal sensor configuration for ultrasonic guided-wave inspection based on value of information, Mech. Syst. Sig. Process. 135 (2020), 106377.
[50] A. Stawiarski, A. Muc, On transducers localization in damage detection by wave propagation method, Sensors 19 (8) (2019) 1937.
[51] C. Fendzi, J. Morel, M. Rebillat, M. Guskov, N. Mechbal, G. Coffignal, Optimal sensors placement to enhance damage detection in composite plates, 2014.